Radiation-Resistant Behavior of Poly(vinylidene fluoride)/Layered Silicate Nanocomposites

Vimal K. Tiwari,[†] Pawan K. Kulriya,[‡] Devesh K. Avasthi,[‡] and Pralay Maiti*[,†]

School of Materials Science and Technology, Institute of Technology, Banaras Hindu University, Varanasi 221 005, India, and Inter University Accelerator Centre, Aruna Asaf Ali Marg, New Delhi 110 067, India

ABSTRACT Poly(vinylidene fluoride) (PVDF) has been made radiation-resistant through a nanocomposite (NC) route. The bombardment of high-energy swift heavy ions (SHI) on PVDF and its NCs with layered silicate has been studied in a range of fluences. The degradation of PVDF after SHI irradiation is suppressed radically in NCs. PVDF forms an intercalated nanostructure in the presence of nanoclay and, further, the ion fluence raises the extent of intercalation. The crystallinity and the heat of fusion of pristine PVDF have drastically been reduced after SHI irradiation, while there are relatively small changes in NCs even at higher fluences. The *metastable* piezoelectric β form of PVDF gets stabilized by the presence of layered silicate, and the structure is retained upon SHI irradiation. The clay platelets act as nucleating agents, and SHI irradiation causes two crystallization temperatures for the samples exposed to high fluences. The damages created on the surface and bulk of PVDF and its NC films upon SHI irradiation have been measured quantitatively by using atomic force microscopy. The pitting dimensions and degradation are enhanced significantly beyond 10^{11} ions/cm^2 fluence for pristine PVDF, which limits the use of PVDF for any ion irradiation application. The degradation is considerably suppressed in NCs, providing a suitable high-energy radiation-resistant thermoplastic polymer.

KEYWORDS: PVDF • nanocomposites • swift heavy ions • structure • morphology • thermal properties

INTRODUCTION

The irradiation of polymeric materials by swift heavy ions (SHI), with energy ≥ 1 MeV/nucleon, leads to remarkable changes in their chemical and physical properties (1, 2). The number of ions per unit area, so-called *fluence*, dictates changes in the chemical, crystalline structure and the physical properties of the polymer, e.g., formation of bonds (3), cross-linking (4), grafting (5), molecular emission (6−8), chain scission, ordering (9), recrystallization (10), amorphization, and latent track (11−13) in the polymer matrix. At low ion fluence, the polymer recrystallizes, while at higher fluence, degradation occurs. The irradiation of SHI on the polymer can induce damage zones along its path and form a latent track due to its large electronic energy deposition. The track diameter depends on the mass and energy of the ions. The latent track, being amorphous in nature, can be used to initiate a phase transformation that modifies, removes, or grafts materials along the channel. The track-etched polymer membranes are of great interest for technological applications (14, 15). The high-energy heavy ion beams are used to irradiate thin polymeric films to produce micro- and nanofilters and biomembranes with high selectivity and controlled permeability. However, the advantages of SHI with respect to a low-energy ion beam are that one cannot expect the desired physical and chemical changes as mentioned above with low-energy ion irradiation.

Poly(vinylidene fluoride) (PVDF) is known to have high chemical stability toward acids and bases and to be mechanically strong, an insulator, and a ferroelectric material. PVDF forms a wide variety of crystalline structures (16−21): among them the β form exhibits piezo- and pyroelectric properties. Therefore, it has versatile technological importance including sensors and actuators (22−24). The β form can usually be obtained from melt crystallization (25) at high pressure, application of a strong electric field (26), and molecular epitaxy on the surface of potassium bromide (27). A PVDF/layered silicate nanocomposite (NC) was first prepared by Priya and Jog (28) using melt compounding, showing the growth of the β form and its improved mechanical properties as compared to those of a pristine polymer. Recently, Shah et al. explored the structural and morphological aspects and toughening of PVDF in bulk in the presence of a few weight percentages of nanometer-sized layered silicate (29, 30). Therefore, PVDF can be prepared for technologically important the β form in bulk by using layered silicate and have strong potentials for its end use in electromechanical devices, gas barriers, membranes, etc.

The interaction of high-energy radiation with PVDF and other fluoro copolymers causes various chemical and physical changes depending on the type of radiation, e.g., electron, plasma, γ irradiation, and SHI. The radiation mainly results in chain scission, cross-linking, and the formation of volatile products (31). Electron irradiation causes an exceptionally high electrostrictive response, exhibiting a typical relaxor ferroelectric behavior in a fluoro polymer (32).

* To whom correspondence should be addressed: E-mail: pmaiti.mst@itbhu.ac.in.
Received for review September 8, 2008 and accepted October 27, 2008
[†] Banaras Hindu University.
[‡] Inter University Accelerator Centre.
DOI: 10.1021/am800040q

Proton irradiation creates different types of radicals in PVDF chains (33). A low dose of γ irradiation (34) induces the crystallinity and gel fraction in PVDF by chain cleavage. The SHI have a set of advantages of generating latent track, which can create nanopores after suitable etching and can act as membrane materials. It has some limitations because PVDF degrades at higher fluence. Therefore, there is a need to develop some composite of PVDF, so that it can be used at higher fluences as well. Further, the effect of SHI on pure PVDF has been reported in the literature (6, 10, 11, 13), causing grafting, cross-linking, and latent track formation in the matrix. So far, there is no report of the effect of SHI irradiation on PVDF/layered silicate NCs.

In this article, we report PVDF as a high-energy resistant material by preparing its NCs with a few weight percentages of layered silicate. The main objective is to study the effect of SHI irradiation on PVDF and its NCs with respect to their nanostructure, structure, morphology, and thermal behavior. The development of a nanostructure, upon SHI irradiation, has been modeled as a function of the nanoclay content in the composite. The present study reveals the radiation-resistant nature of PVDF/layered silicate NC thin films.

EXPERIMENTAL SECTION

Materials. A commercial PVDF (SOLEF 6008; Ausimont, Italy), with a melt flow index of 24 g/10 min at 230 °C under a 5 kg load, was used in this work. An organically modified clay, Cloisite 30B [bis(hydroxyethyl)methyl tallow ammonium ion exchanged montmorillonite], purchased from Southern Clay Products Inc. (Gonzales, TX), was used as the nanofiller. Tallow is a mixture of C_{18} and C_{16} long-chain alkenes. After the organic modification, the gallery spacing increases to 1.8 nm from 1.1 nm spacing of unmodified clay. The lateral dimension of nanoclay is ~250 nm.

Preparation of NCs. Initially, the PVDF beads were converted into powder form by using a home-built chip sizer. Requisite amounts of PVDF powder and nanoclay (4 and 8 wt %) were mixed well in a high-speed (1000 rpm) mixer before putting it into the extruder. The NCs were prepared by a melt extrusion method. Extrusion was carried out in a twin-screw extruder (Hakke Mini Lab). The mixing was done at a temperature of 205 °C for 10 min under the shear rate of 100 rpm. Henceforth, the PVDF NCs will be designated as "NC4" and "NC8" for 4 and 8 wt % of nanoclay in the polymer matrix, respectively. Both the extruded strips (NCs) and pure PVDF were melt-pressed into a thin film of ~30 μm thickness of size 1 × 1 cm^2, in a compression-molding machine at 190 °C under 5 tons of pressure for irradiation of SHI.

SHI Irradiation. PVDF and its NCs were irradiated by a 80 MeV Si^{7+} ion in a vacuum of ~10^{-6} Torr at Inter University Accelerator Centre, New Delhi, India. To avoid heating effects, the beam current was maintained at 0.5 pnA (particles nanoampere) with a spot size of 2 × 2 mm^2. The ion beam was scanned by an electromagnetic scanner in the area of 1 × 1 cm^2. The ion fluence range was kept between 10^{10} and 10^{13} ions/cm^2. The electronic energy loss (S_e) was ~2.44 keV/nm. whereas the nuclear energy loss was ~1.9 eV/nm, as estimated by SRIM simulation (35). Both the PVDF and the NCs were irradiated with 80 MeV Si^{7+} at various fluences. The thickness of the thin film and energy of the Si^{7+} ions were chosen in such a way that the range (distance covered by the particles with that initial kinetic energy) of the ions is greater than the film thickness to ensure that no ion will be implanted rather than passed through the thin film.

X-ray Diffraction (XRD). XRD experiments were performed using a Bruker AXS D8 Advance wide-angle X-ray diffractometer with Cu Kα radiation and a graphite monochromator (wavelength, $\lambda = 0.154$ nm). The generator was operated at 40 kV and 40 mA. Thin films of pure PVDF and NC samples (before and after ion irradiation) were placed on a quartz sample holder at room temperature and were scanned at diffraction angle 2θ from 1° to 40° at a scanning rate of 1°/min to explore the nanostructure and crystalline structure of pure PVDF and, thereby, the effect of the nanoclay on the structure, before and after ion irradiation.

Differential Scanning Calorimetry (DSC). The melting temperature, crystallization temperature, and heat of fusion of irradiated and freshly prepared NC and pure PVDF thin films were measured in a Mettler 832 DSC instrument. The samples were heated at a scan rate of 10 °C/min. The peak temperature and enthalpy of fusion were measured from the endotherm using a computer attached with the instrument. After the first melting, the samples were cooled down at a constant rate of 10 °C/min to find the crystallization temperature and heat of crystallization in a similar fashion. Further, a second heating was taken to ensure the amount of crystallinity and melting temperature after removal of all of the thermal history in the first run. The cooling rate dependence on the crystallization behavior was studied with variable cooling rates from 5 to 20 °C/min. The DSC was calibrated with indium and zinc before use.

Morphological Investigation. The morphology of the thin film of pure PVDF and NCs (both irradiated and pristine) was investigated by using scanning electron microscopy (SEM) and atomic force microscopy (AFM). The surface morphology of the thin film was examined with a LEO 435VP instrument operated at 15 kV. All of the samples were gold-coated by means of a sputtering apparatus before observation. A NT-MDT multimode atomic force microscope, Russia, controlled by a Solver scanning probe was used for the surface morphology study. A semicontact mode was used, with the tip mounted on a 100-μm-long single-beam cantilever with a resonant frequency in the range of 240−255 kHz and a corresponding spring constant of 11.5 N/m. A thin film of ~30 μm was used for AFM studies for both PVDF and NCs, before and after irradiation. The average of the individual pitting diameter and depth was measured from around 20 separate pittings in the AFM micrographs. Transmission electron microscopy (TEM) was used to observe the nanoscale dispersion of the nanoclay in the matrix polymer. TEM images were obtained using a Philips CM-10 instrument operated at an accelerating voltage of 100 kV. A thin layer was sectioned at −80 °C using a Leica ultracut UCT equipped with a diamond knife.

RESULTS AND DISCUSSION

Figure 1 shows the optical photographs of pure PVDF and its NC before and after SHI irradiation. Pure PVDF turns completely black/charred in a fluence of 10^{12} ions/cm^2. In fact, it has started getting black/charred at around a 10^{11} fluence and becomes brittle at a 10^{13} fluence. The remarkable thing is that NC4 becomes slightly brownish at the same high fluence. Pure PVDF degrades at higher fluence, which is obvious for any organic polymer that undergoes chain scission upon SHI irradiation, while the degradation of PVDF has significantly been suppressed in NC4 in the presence of a few weight percentages of nanoclay. It has to be noted that NC4 shows a slight color even before SHI irradiation, arising from dispersion of the nanoclay during the extrusion process. The dispersion of nanoclays in the matrix PVDF, as is evident from the TEM image in Figure 2, protects PVDF from

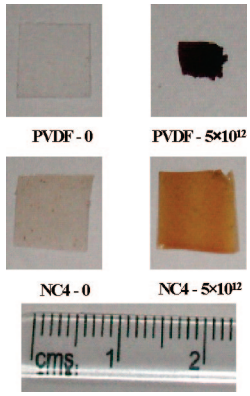

FIGURE 1. Optical micrographs of PVDF and its NC (NC4) with indicated fluence. The pristine PVDF and NC4 have been indicated by "0". The scale has been given to show the dimension of the film used for irradiation. A part of the PVDF at 5×10^{12} fluence has been placed because it was very brittle and broken during recovery of the sample from the ladder.

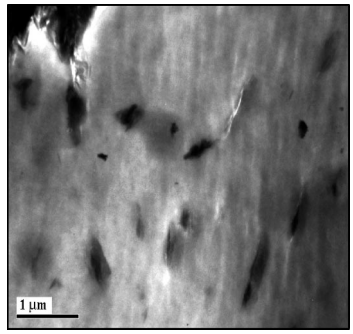

FIGURE 2. Bright-field TEM image of PVDF NC (NC4) before irradiation.

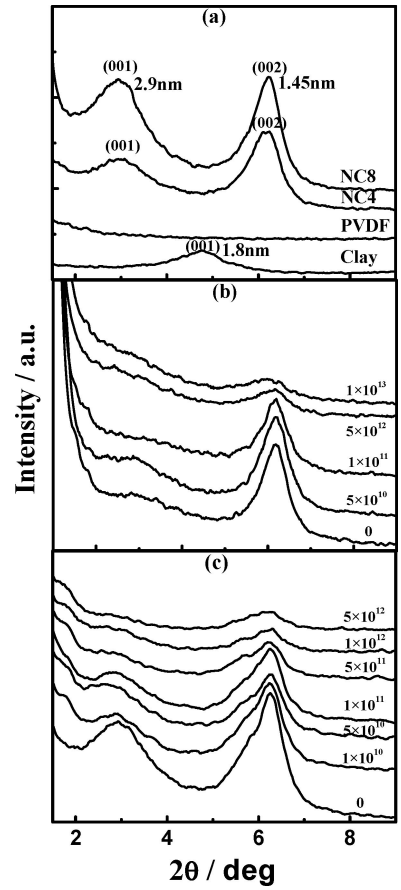

FIGURE 3. Wide-angle XRD patterns of (a) organically modified clay, pure PVDF and its NCs before irradiation. XRD patterns of the NCs at various fluences: (b) NC4; (c) NC8. The number "0" indicates the zero fluence or pristine polymer (before irradiation).

its degradation during SHI irradiation. This is the first report of the new advantage of a nanoparticle dispersed in the polymer matrix, where the nanoparticles protect the polymer matrix from high-energy SHI irradiation.

Figure 3a shows the XRD patterns of an organically modified nanoclay, pristine PVDF, and their NCs, showing their nanostructure at lower angle. The (001) peak, intergallery spacing of an organically modified nanoclay at $2\theta = 4.9°$, corresponds to the layer spacing of 1.8 nm, while the same peak has been shifted to a lower angle ($2\theta = 3.0°$) for NCs with a gallery spacing of 2.9 nm. The gallery spacing increases by more than 1 nm in NCs as compared to a pure nanoclay: exhibiting intercalation of polymer chains inside the silicate layers. However, pristine PVDF does not show any nanostructure in the lower angle studied. The stronger peak at $2\theta = 6.1°$ is due to the (002) peak of layered silicates. The (002) peak is usually less intense than that of the (001) peak. The stronger peak is presumably due to the coexistence of the (002) clay peak along with the interplanar distance of an aligned PVDF chain inside the gallery. Parts b and c of Figure 3 show the nanostructures of NC4 and NC8 as a function of the fluence. The (001) peak of NC4 is not as prominent as that in the thick film (Figure 3a), presumably because of the preferred orientation during melt pressing to prepare the thin film because the clay content is less. However, the peak has been shifted to a lower angle with an increase in the fluence, indicating a higher gallery spacing for NC4 upon SHI irradiation. The (001) peak of NC8 is quite prominent even in the thin film because the coherency of the silicate stacks is sufficient in the presence of a higher clay content. Interestingly, we found two peaks after SHI irradiation in NC8. The gallery spacing (d_{001}) has been plotted with the fluence in Figure 4. The horizontal dotted line indicates the gallery spacing of the unirradiated NCs. Clearly, the spacing enlarges with an increase in the fluence. During irradiation, each ion creates a cylindrical molten zone of a few nanometers, transiently along its path, during which the temperature of the sample is quite high (~500 °C) and the low viscous polymer has enough time to diffuse into the gallery to cause higher intercalation. It has to be mentioned here that the higher the fluence, the higher is the time of SHI exposure. So, the polymer gets more time to *diffuse-in* inside the gallery at higher fluence (36). Nonetheless, intercalation of the polymer gradually increases with the fluence. After irradiation, the polymer gets quenched, being in contact with the metal ladder and usually trying to crystallize at the earliest. After crystallization, the polymer chains cannot diffuse-in inside the nanoclay layers. Therefore, the nanostructures of the irradiated NCs are what they develop during SHI irradiation. The low-angle peaks (~1.8°) of NC8 (Figure 3c), which appear only after SHI irradiation, are explained from the greater intercalation of the polymer in and around the point of SHI irradiation, where the kinetic

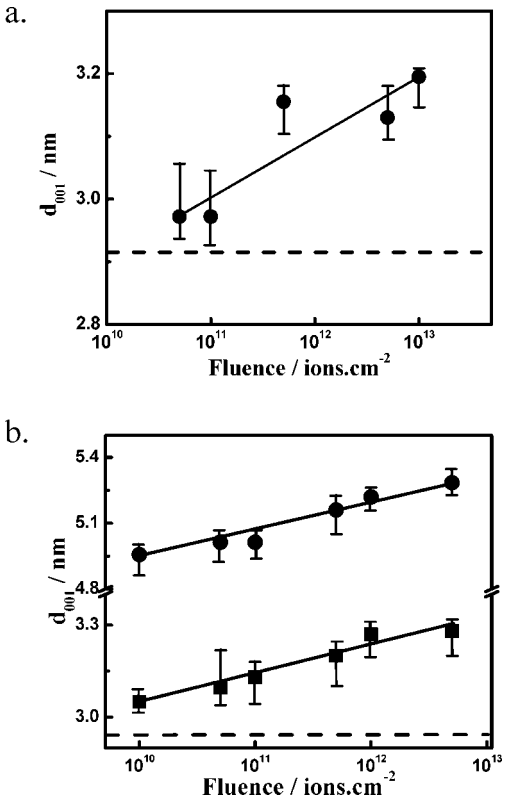

FIGURE 4. Intergallery spacing as a function of the fluence: (a) NC4; (b) NC8. The dashed lines represent the spacing before irradiation. The closed circles are calculated from the lower angle peak position from Figure 3 for NC8 in part b, while the closed squares are calculated from the intermediate peak (~3°).

energy of the polymer is expected to be high; as a result, the extent of intercalation is further enhanced. The zones away from SHI irradiation have the diffuse effect of the thermal energy and provide the peak at ~3° of NC8. Both peaks of NC8 exhibit fluence dependency, and the corresponding gallery spacing increases with an increase in the fluence (Figure 4b). The phenomenon has been modeled in Scheme 1 to show the different locations of the matrix exposed to SHI bombardment. The effect should be manifested in NC4 as well, but because of the lower coherency of the (001) plane, the peak intensity is too low to detect. However, SHI irradiation originates further intercalation of sufficient polymer inside the nanoclay gallery.

Parts a–c of Figure 5 show XRD patterns (crystalline structure) of pristine PVDF and NCs as a function of the fluence. As usual, melt-quenched pure PVDF crystallizes in the α form (37, 38). The structure remains the same with an increase in the fluence, but the intensity of the crystalline peaks gradually decreases, indicating amorphization of PVDF after SHI irradiation. On the contrary, PVDF crystallizes in the β form (28) in the presence of nanoclay in NC4 and NC8, and interestingly moderately strong β peaks exist even at very high fluence. Here also, it is clear that PVDF in NCs can retain its structural integrity even at higher fluence, while pristine PVDF degrades, showing relatively weak crystalline peaks upon SHI irradiation. The intensity of the (020) plane has significantly been reduced in pure PVDF, and the decreasing trend persists with an increase in the fluence,

Scheme 1. Schematic View of the Intercalation at Different Parts of the Sample Leading to Two Different Gallery Spacings[a]

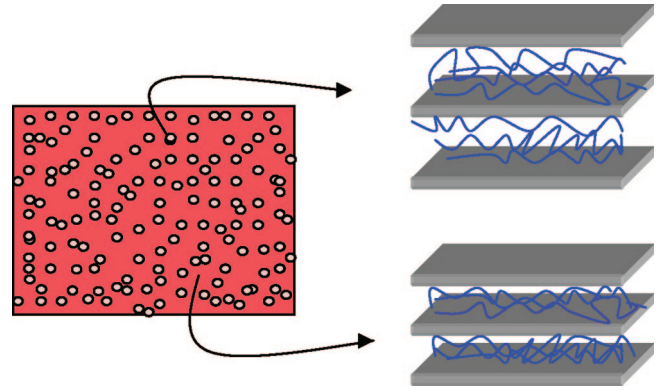

[a] The circles are the spot where bombardment of SHI occurred. The upper intercalation represents in and around the point where bombardment occurs and lower intercalation arising from the zones away from the bombardment points.

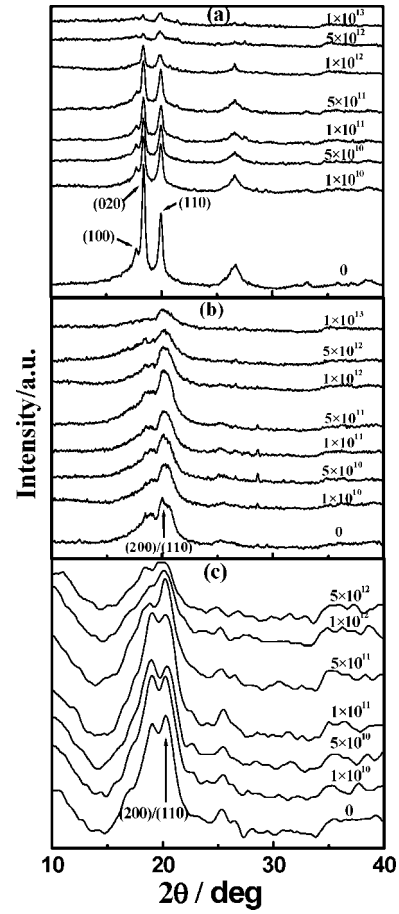

FIGURE 5. Wide-angle XRD patterns of (a) pure PVDF, (b) NC4, and (c) NC8 at indicated fluences. The number "0" indicates the zero fluence or pristine polymer (before irradiation).

while there is only a slight reduction in the intensity of the (200)/(110) plane of NCs. The high-energy SHI irradiation initially melts the pure PVDF matrix and then degrades/cross-links most of the polymer chains. The degraded and/or cross-linked PVDF molecules cannot crystallize further and, hence, exhibit lower intense peaks in XRD patterns. The matrix PVDF melts after SHI irradiation in NCs, but there is

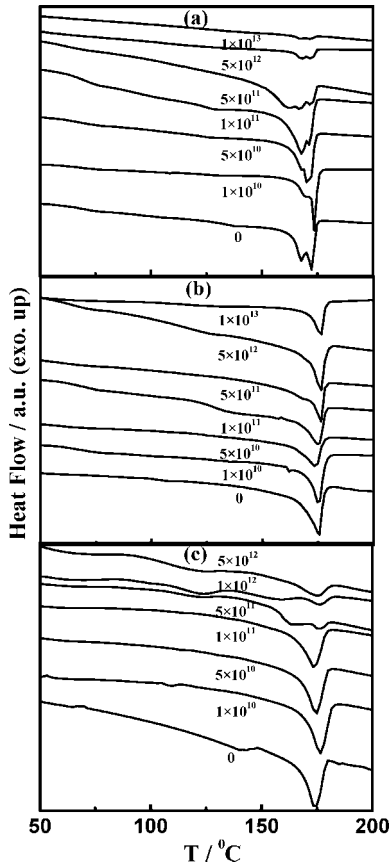

FIGURE 6. DSC thermograms of (a) pure PVDF, (b) NC4, and (c) NC8 at indicated fluences during the first heating at a heating rate of 10 °C/min.

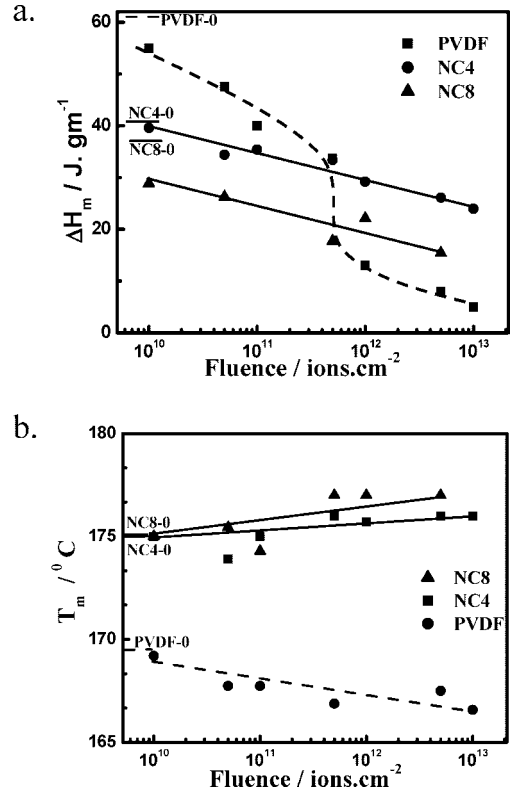

FIGURE 7. (a) Heat of fusion and (b) melting temperature as a function of the fluence for pure PVDF and NCs. The solid and dashed lines are guides to the eye. The small horizontal solid and dashed lines are the values for the corresponding pristine samples indicated as "0".

no significant degradation. As a result, it recrystallizes in the same β form when SHI irradiation stops. However, XRD results show that PVDF is affected marginally upon SHI irradiation in the presence of a few weight percentages of organically modified nanoclay.

The DSC thermograms of PVDF and NCs are shown in Figure 6a–c, before and after SHI irradiation with different fluences. Pure PVDF shows double melting, as reported in the literature, and the peak of the main melting endotherm, T_m, decreases with an increase in the fluence (169.2 and 166.6 °C for pristine and 10^{13} ions/cm^2 fluence irradiated samples, respectively). Another feature is that the area under the whole melting curve, known as the heat of fusion (ΔH), gradually decreases with an increase in the fluence for pure PVDF. On the contrary, T_m and ΔH do not change significantly with the fluence for NCs. The ΔH values are plotted against the fluence in Figure 7a. Initially, the ΔH values decrease gradually with an increase in the fluence for pure PVDF, and then a drastic change occurs at 5×10^{11} fluence, beyond which PVDF shows a very low heat of fusion (<10 J/g). In contrast, there is relatively less reduction in ΔH with an increase in the fluence for NCs. The amorphization/degradation of pure PVDF is severe after 1×10^{11} fluence, as is evident from the damage of films; as a result, there is a significant reduction in ΔH, while the degradation is somehow restricted in NCs, causing similar heats of fusion even for specimens exposed to higher fluence. Because $\Delta H°$, heat of fusion for 100% β-PVDF, is not known in the literature, we have plotted the heat of fusion instead of the percentage crystallinity. However, there is a decrease in ΔH of the irradiated specimen as compared to the unirradiated one for both PVDF and NCs because of SHI collisions, but the effect on the NCs is certainly limited. The melting temperatures, T_m, of pure PVDF and NCs are shown in Figure 7b, exhibiting a significant decreasing tendency for pure PVDF and a slight increasing tendency for NCs, which also emphasizes severe amorphization in pure PVDF and insignificant changes in NCs. The cooling curves in DSC, both before and after irradiation, are presented in Figure 8a,b. The crystallization occurs at ~140 °C in a single isotherm for pure PVDF irrespective of the fluence. In contrast, NC4 crystallizes at 147 °C, 7 °C higher as compared to that of pure PVDF, and further the crystallization temperature (T_c) increases up to 150 °C with an increase in the fluence. At 10^{11} fluence, a shouldering at lower temperature arises and becomes prominent with an increase in the fluence. The lower T_c is around 140 °C, exactly the same T_c as that of pure PVDF. The nanoclay acts as a good nucleating agent and, therefore, explains well the increase of T_c for NC4 as compared to that of pure PVDF before irradiation. After SHI irradiation, the degree of intercalation is enhanced and, thereby, the proximity of the polymers with the inorganic surface of the clay layers increases, causing higher T_c values of irradiated NC4 at lower fluence. Moreover, at higher fluence, greater than 10^{11} ions/cm^2, the appearance of lower

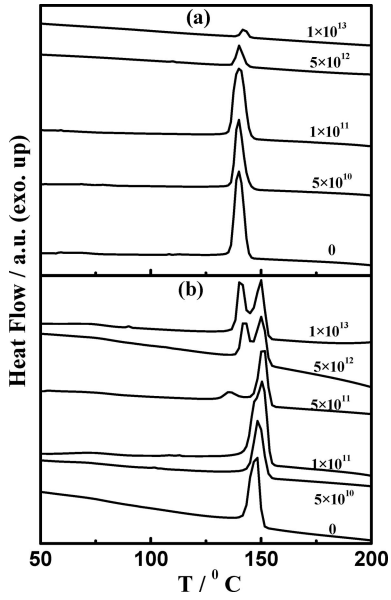

FIGURE 8. DSC thermograms of (a) pure PVDF and (b) NC (NC4) at indicated fluences during cooling at a scan rate of 10 °C/min.

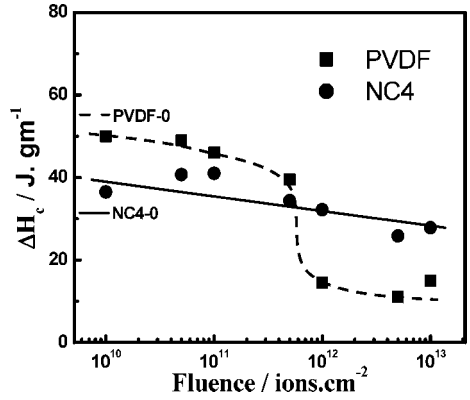

FIGURE 9. Heat of crystallization against fluence for pure PVDF and NC (NC4). The solid and dashed lines are guides to the eye. The small horizontal solid and dashed lines are the values for the corresponding pristine samples.

T_c values is presumably because of the segregation of layered silicate to a greater extent predominantly because of amorphous ion tracks created by ions passing through the NC matrix. At high fluence, the time of melt state is long, and during that time, the kinetic motion of SHI can orient the layered silicate in the liquid polymer, generating a layered-silicate-free amorphous zone, which may provide a crystallization temperature during cooling very similar to that of pure PVDF at 140 °C and the T_c values of the nanoclay-rich zones exhibited at a higher temperature region. Figure 9 shows the heat of crystallization (ΔH_c) as a function of the fluence during cooling in DSC. Pure PVDF shows very low ΔH_c values at higher fluence, which confirms the nonavailability of crystallizable polymer chains as a result of SHI-induced degradation. The NCs show a slight decrease in the ΔH values of the entire fluence range studied here. The second meltings of both PVDF and NC4 also show similar trends like their first melting behavior including the heat of fusion and are presented in the Supporting Information (Figures S1 and S2). The thermal behavior proves that pure

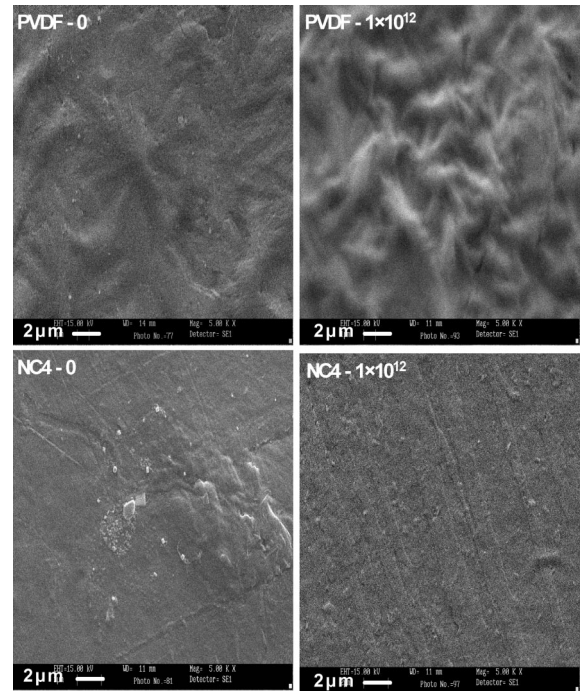

FIGURE 10. SEM images of PVDF and NC4 surfaces before and after the indicated ion irradiation. The number "0" indicates zero fluence (before irradiation).

PVDF degrades upon SHI irradiation, while the degradation behavior is suppressed in NC in the presence of nanoclay. Now, it is pertinent to discuss the cause of this protection of the matrix in the presence of nanoclay. There are two possibilities: (1) nanoclay, being ceramic in nature and having a lateral dimension ~250 nm well dispersed in the polymer matrix, can protect the polymer from SHI irradiation and (2) the modified β form in the presence of clay can also be SHI-resistant.

The Fourier transform infrared (FTIR) studies also confirm the existence of the β form of PVDF in the presence of nanoparticles in NCs, as is evident by the peaks at 510 and 840 cm^{-1} in the Supporting Information (Figure S3a–c) (20). The intensities of α-crystalline peaks at 490, 615, 763, and 976 cm^{-1} reduce with an increase in the fluence, which indicates that the crystallinity decreases as a result of SHI irradiation. On the other hand, the β-crystalline peaks in NCs are quite strong even at higher fluence, as shown in the figure. The FTIR results also support the amorphization of pure PVDF upon SHI irradiation, as compared to NCs. The switchover of the structure from α to β is also reflected in polarizing optical micrographs [Supporting Information (Figure S4)]. The α form in pure PVDF shows compact spherulite, while the birefringence is completely missing in the β form of PVDF in NCs because of the meshlike structure (29).

The surface morphology of PVDF and NCs, before and after SHI irradiation, are shown in SEM images in Figure 10. As usual, the spherulitic morphology is apparent in pure PVDF (29, 39) before irradiation, while the distorted morphology appeared after SHI irradiation. The SHI destroy the spherulitic morphology of PVDF. In contrast, the meshlike morphology was apparent in NCs (29) before SHI exposure, which does not change even after the high fluence of SHI

irradiation. This clearly shows that SHI have very little effect on the NC film surfaces, whereas pure PVDF surfaces get damaged by SHI bombardment. Moreover, a striation observed in the NC film after SHI exposure might be due to the segregation of the amorphous and crystalline zones.

The surface morphology was further explored by means of AFM, and the three-dimensional images of PVDF and NC4 are presented in the Supporting Information (Figure S5) for various fluences. Both PVDF and NC4 show comparatively smooth surfaces before SHI irradiation. The PVDF surface gets damaged with an increase in the fluence, and large pittings are found at higher fluence (5×10^{12} ions/cm^2). In contrast, there is a slight damage in the NC4 surface in that similar fluence. Two-dimensional AFM images of pristine PVDF and NC4 are shown in the Supporting Information (Figure S6), which also exhibits bigger pittings in the case of pure PVDF, while NC4 shows only limited pitting with smaller size. The attached scale can be a measure of the pitting dimension. In order to compare the individual pitting sizes, we struck out one single pitting, which is shown in the Supporting Information (Figure S7) with its relative shape and size. Both the pitting diameter and depth have been broadened after SHI exposure in pure PVDF, while a minimum increase in the size of the pittings was observed for NCs. The real shape and size of an individual pitting (*inverted crater*) have been measured by using the AFM Solver program and are presented quantitatively in the Supporting Information (Figure S8). The diameter of an irradiated PVDF pitting has broadened more than an order of magnitude (from 0.3 μm to 4.0 μm) and the corresponding depth has increased 6-fold, as compared to those of pristine PVDF. Conversely, the pitting diameter and depth of SHI-irradiated NC4 have increased 2 and 1.5 times, as compared to those of pristine NC4, respectively. The pittings are usually considered as a measure of roughness. Then, before exposure, the roughnesses of pure PVDF and NC were similar (the pitting diameter and depth are almost the same), but after SHI irradiation, 8- and 4-fold increases in the depth and diameter of pure PVDF were observed, respectively, as compared to those of NC4. Obviously, the pitting size is more in pure PVDF as a result of severe degradation in the matrix after SHI irradiation. Figure S8 in the Supporting Information is the case of an individual pitting. In order to get a standard picture, we have measured around 20 pittings from each sample and then averaged the pitting dimensions (both the depth and diameter), and the results are presented in Figure 11a,b. The average diameter of the pittings increased very fast with an increase in the fluence for PVDF (Figure 11a), while it nominally increased in NC in the same fluence range, indicating a suppression of damage in NCs in the presence of nanoparticles even after SHI irradiation. The pitting depth also increases drastically for pure PVDF, but there is only a slight increase in NC4 (Figure 11b). Both the average pitting diameter and depth clearly indicate that the SHI can damage pure PVDF easily, while the matrix polymer is being protected from high-energy SHI in NCs in the presence of nanoclay.

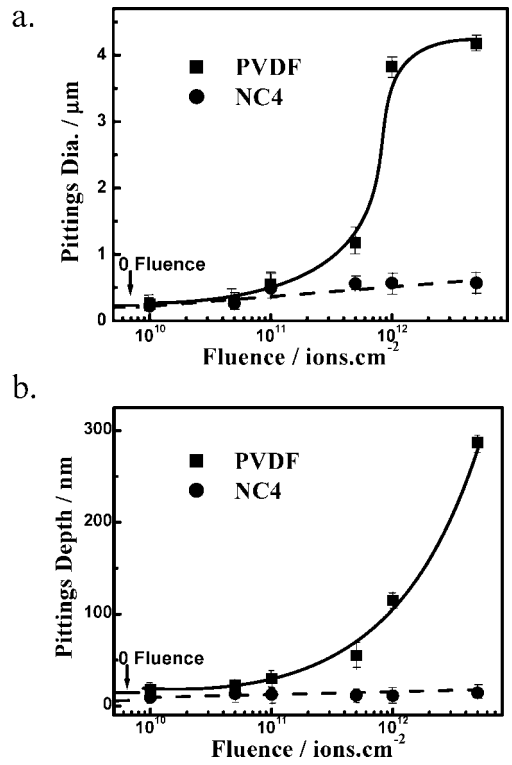

FIGURE 11. Average dimension of pitting in PVDF and NC4 from AFM images: (a) pitting diameter and (b) pitting depth of PVDF and NC4 at various fluences. The small horizontal lines represent the values for respective pristine samples.

All of the above experiments clearly show that a few percentages of layered silicate dispersed in PVDF can protect the matrix from irradiation of high-energy SHI. Thus, PVDF NCs can be used as radiation-resistant materials. One can enhance the intercalation with the desired level by bombarding SHI on polymer/layered silicate NCs using suitable fluences. The extent of intercalation dictates the ultimate properties, e.g., mechanical strength, etc., of the polymer NCs. The same idea can be extended to other thermoplastics or engineering plastics. Other potential uses of irradiated PVDF NCs can be in a fuel cell membrane, where both the strength and the right kinds of porosities are required. One can generate ion tracks of different dimensions by irradiating SHI into a polymeric substrate followed by a suitable etching technique. We are continuing work in that direction as well. However, the polymer NCs can provide a high-energy radiation-resistant material.

CONCLUSION

The SHI beyond 10^{12} ions/cm^2 fluence degrade pure PVDF, while the dispersion of a few weight percentages of nanoclay in NC protects the matrix from degradation, with a clue for a possible potential use of thermoplastics as radiation-resistant material arising. PVDF in layered silicate forms an intercalated nanostructure, and the extent of intercalation increases with an increase in the fluence. Pure PVDF almost amorphizes under SHI irradiation, whereas the crystallinity has slightly been reduced in NCs even after high fluence SHI irradiation, as is evident from optical images and XRD, DSC, and FTIR analyses. The nanoclay acts as a

nucleating agent, as is obvious from the higher temperature of crystallization, and SHI irradiation promotes segregation of the layered silicate during bombardment, hence giving two temperatures of crystallization due to pure PVDF and nanoclay-induced crystallization. The surfaces, including spherulitic morphology, gets damage pure PVDF after SHI irradiation, but it is unaffected in NCs. The shape and size of the pittings formed as a result of SHI irradiation have been explored and compared for PVDF and NCs. Both the pitting depth and diameter increase significantly, leading to catastrophic degradation in pure PVDF, while nanoclay resists that degradation, showing almost the same pitting dimensions as those of pristine NCs.

Acknowledgment. The authors acknowledge the receipt of research funding and peletron source from Inter University Accelerator Centre, New Delhi, India (Project IUAC/XIII.7/UFUP-3932/5603). The authors also acknowledge Dr. Asish Lele and Dr. S. Sinha Ray for extrusion work and TEM studies, respectively, and Ausimont, Italy, for supplying PVDF samples.

Supporting Information Available: Figures S1−S10. This material is available free of charge via the Internet at http://pubs.acs.org.

REFERENCES AND NOTES

(1) Venkatesan, T.; Calcagno, L.; Elman, B. S.; Foti, G. In *Ion Beam Modification of Insulators*; Mazzoldi, P.; Arnold, G. W., Eds.; Elsevier: Amsterdam, The Netherlands, 1987; Vol. 2.
(2) Sasuga, T.; Kawanishi, S.; Seguchi, T.; Kohno, I. *Polymer* **1989**, *30*, 2054.
(3) Betz, N. *J. Polym. Sci.* **1994**, *32*, 1493.
(4) Daudin, B.; Legrand, J. F.; Macchi, F. *J. Appl. Phys.* **1991**, *70* (8), 4037.
(5) Mazzei, R. O.; Bermudez, G. G.; Tadey, D.; Rocco, C. *Nucl. Instrum. Methods Phys. Res., Sect. B* **2004**, *218*, 313.
(6) Torrisi, L.; Percolla, R. *Nucl. Instrum. Methods Phys. Res., Sect. B* **1996**, *117*, 387.
(7) Torrisi, L.; Ciavola, G.; Foti, G.; Percolla, R. *Nucl. Instrum. Methods Phys. Res., Sect. A* **1996**, *382*, 361.
(8) Mittal, V. K.; Lotha, S.; Avasthi, D. K. *Radiat. Eff. Defects Solids* **1999**, *147*, 199.
(9) Percolla, R.; Calcagno, L.; Foti, G. *Appl. Phys. Lett.* **1994**, *65* (23), 2966.
(10) Biswas, A.; Gupta, R.; Kumar, N.; Avasthi, D. K.; Singh, J. P.; Lotha, S.; Fink, D.; Paul, S. N.; Bose, S. K. *Appl. Phys. Lett.* **2001**, *78* (26), 4136.
(11) Zagorski, D. L.; Vilensky, A. I.; Kosarev, S. A.; Miterev, A. M.; Zhdanov, G. S.; Mchedlishvih, B. V. *Radiat. Meas.* **2003**, *36*, 233.
(12) Oganessian, V. R.; Trofimov, V. V.; Vetter, J.; Danziger, M.; Dorschel, B.; Hermsdorf, D. *Nucl. Instrum. Methods Phys. Res., Sect. B* **2003**, *208*, 166.
(13) Szenes, G. *Nucl. Instrum. Methods Phys. Res., Sect. B* **1999**, *155*, 301.
(14) Vijay Y. K. *Int. J. Hydrogen Energy* **2007**.
(15) Kulshrestha, V.; Awasthi, K.; Vijay, Y. K. *Int. J. Hydrogen Energy* **2007**.
(16) Tazaki, M.; Wada, R.; Okabe, M.; Homma, T. *J. Appl. Polym. Sci.* **1997**, *65*, 1517.
(17) Hasegawa, R.; Kobayashi, M.; Tadokoro, H. *Polym. J.* **1972**, *3*, 593.
(18) Hasegawa, R.; Takahashi, Y.; Chatani, Y.; Tadokoro, H. *Polym. J.* **1972**, *3*, 600.
(19) Lando, J. B.; Olf, H. G.; Peterlin, A. *J. Polym. Sci., Part A-1* **1969**, *4*, 941.
(20) Kobayashi, M.; Tashiro, K.; Tadokoro, H. *Macromolecules* **1975**, *8*, 158.
(21) Basset, D. C. In *Development in Crystalline Polymers*; Basset, D. C., Ed.; Applied Science Publishers: London, 1982.
(22) Stobener, U.; Gaul, L. *J. Intell. Mater. Syst. Struct.* **2001**, *11* (4), 283.
(23) Lee, C. S.; Joo, J.; Han, S.; Koh, S. K. *Appl. Phys. Lett.* **2004**, *85* (10), 1841.
(24) Khanna, P. K.; Hornbostel, B.; Grimme, R.; Schaefer, W.; Dorner, J. *Mater. Chem. Phys.* **2004**, *87* (1), 173.
(25) McGrath, J. C.; Ward, I. M. *Polymer* **1980**, *21*, 855. Tamura, M.; Ogasawara, K.; Ono, N.; Hagiwara, S. *J. Appl. Phys.* **1974**, *45*, 3768.
(26) Scheinbeim, J.; Nakafuku, C.; Newman, B. A.; Pae, K. D. *J. Appl. Phys.* **1979**, *50*, 4399. Newman, B. A.; Yoon, C. H.; Pae, K. d.; Scheinbeim, J. *J. Appl. Phys.* **1978**, *49*, 4601.
(27) Lovinger, A. J. *Polymer* **1981**, *22*, 412.
(28) Priya, L.; Jog, J. P. *J. Polym. Sci., Part B: Polym. Phys.* **2002**, *40*, 1682. (a) Priya, L.; Jog, J. P. *J. Polym. Sci., Part B: Polym. Phys.* **2003**, *41*, 31.
(29) Shah, D.; Maiti, P.; Gunn, E.; Schmidt, D. F.; Jiang, D. D.; Batt, C. A.; Giannelis, E. P. *Adv. Mater.* **2004**, *16* (14), 1173.
(30) Shah, D.; Maiti, P.; Jiang, D. D.; Batt, C. A.; Giannelis, E. P. *Adv. Mater.* **2005**, *17* (5), 525.
(31) Forsythe, J. S.; Hill, D. J. T. *Prog. Polym. Sci.* **2000**, *25*, 101.
(32) Zhang, Q. M.; Bharti, V.; Zhao, X. *Science* **1998**, *280*, 2101.
(33) Adem, E.; Burillo, G.; Munoz, E.; Rickards, J.; Cota, L.; Avalos-Borja, M. *Polym. Degrad. Stab.* **2003**, *81*, 75.
(34) Zhudi, Z.; Wenxue, Y.; Xinfang, C. *Radiat. Phys. Chem.* **2002**, *65*, 173.
(35) Bersack, J. P.; Haggmark, L. G. *Nucl. Instrum. Methods* **1980**, *174*, 257.
(36) Maiti, P.; Nam, P. H.; Okamoto, M.; Hasegawa, N.; Usuki, A. *Macromolecules* **2002**, *35*, 2042.
(37) Prest, W. M., Jr.; Luca, D. J. *J. Appl. Phys.* **1978**, *49*, 5042.
(38) Gregorio, R., Jr.; Cestari, M. *J. Polym. Sci., Part B: Polym. Phys.* **1994**, *32*, 859.
(39) Maiti, P.; Nandi, A. K. *Macromol. Chem. Phys.* **1998**, *199*, 1479.

AM800040Q